Probing Crustal Anisotropy by Receiver Functions at the Deep Continental Drilling Site KTB in Southern Germany

Bianchi I.*, Bokelmann G.

*irene.bianchi@univie.ac.at

Department of Meteorology and Geophysics, University of Vienna, Austria

Keywords: Anisotropy, Passive method, Shear-wave velocity

Abstract

Seismic anisotropy is a unique observational tool for remotely studying deformation and stress within the Earth. Effects of anisotropy can be seen in seismic data; they are due to mineral alignment, fractures or layering. Seismic anisotropy is linked to local stress and strain, allowing modern geophysics to derive geomechanical properties from seismic data for supporting well planning and fracking.

For unravelling anisotropic properties of the crust, the teleseismic receiver functions (RF) methodology has started to be widely applied recently due to its ability in retrieving the 3D characteristics of the media sampled by the waves. The applicability of this technique is tested here by a field test carried out around the KTB (Kontinental Tiefbohrung) site in Southeastern Germany. We compare our results to previous investigations of the metamorphic rock pile of the Zone Erbendorf-Vohenstrauss, drilled down to 9 km depth, which sampled an alternating sequence of paragneiss and amphibolite, in which a strong foliation has been produced by ductile deformation. The application of the RFs reveals the presence of two distinct anisotropic layers within the metamorphic rock pile at 0 to 4 km and below 6 km depth, with up to 8% anisotropy; the depth of these two layers corresponds to

This article has been accepted for publication and undergone full peer review but has not been through the copyediting, typesetting, pagination and proofreading process, which may lead to differences between this version and the Version of Record. Please cite this article as doi: 10.1111/1365-2478.12883

EAGE Publications B.V., PO Box 59, 3990 DB, Houten, The Netherlands

the location of mica-rich paragneiss which show intense foliation, and finally proves the relation between the signal in the RFs, rock texture and presence of cracks. We have now the capability of providing insights from passive seismic data on geomechanical properties of the rocks, useful for geological exploration and engineering purposes, which will help influencing expensive drilling decisions thanks to future application of this seismic technique.

Keywords: Anisotropy, Passive method, Shear wave velocity

1. Introduction

Seismic anisotropy and its determination is of great interest, since it is a key for constraining preferred alignment of structures within the Earth such as due to sedimentary layering, stress-induced cracks, and/or dykes and sills (Babuška and Cara, 1991), the causes of which include the mechanical stress field and deformation. The receiver functions (RF) are time series composed of P-to-S phases generated at impedance contrasts at depth, and their multiples. Their arrival times depend on both velocity in the crossed medium and depth of the velocity contrast (Ammon, 1990, Langston, 1979). The RF technique has been employed for inferring the presence of anisotropic media in the subsurface layers (e.g Levin and Park, 1998; Girardin & Farra, 1998; Schulte-Pelkum et al., 2005; Licciardi et al. 2018). To fully prove the technique of anisotropic RF, we have established a critical test - a field experiment around the deep drilling site KTB in the Oberpfalz area in Bavaria (Southern Germany, Figure 1a), to reproduce the structural information that has previously been obtained by drilling and the more classical seismic techniques e.g. near-vertical and wide-angle seismics. The crust at the KTB site was indeed explored by means of seismic reflection studies (DEKORP Research Group, 1987; DEKORP Research Group, 1988; Eisbacher et al, 1989; Lüschen et al, 1996; Harjes et al., 1997; DEKORP and Orogenic processes Working Groups, 1999; Muller et al, 1999). The metamorphic body of the Zone of Erbendorf-Vohenstrauss (ZEV) was drilled until reaching a depth of 9101 meters (Harjes et al, 1997 and references therein). The ZEV is made

EAGE Publications B.V., PO Box 59, 3990 DB, Houten, The Netherlands

of an alternating sequence of paragneisses and amphibolites showing a strong foliation. Unexpected though was the steep inclination of that pervasive foliation, which did not correspond to previous interpretations of flat seismic reflections and mapped surface geology (Harjes et al., 1997). Previous tectonic interpretations had to be strongly modified, to explain the in-situ information from the borehole (Emmernann and Lauterjung, 1997; Obrien et al., 1997). Principal results from the drilling and accompanying geophysical experiments are described in a special JGR volume (Haak and Jones, 1997; Emmermann and Wohlenberg, 1989), the KTB borehole is not any longer active.

Cores samples have been used in laboratory tests for determining the seismic velocities and anisotropy (Kern and Schmidt, 1990; Kern et al, 1991; Berckhemer et al., 1997; Zang et al., 1996); vertical seismic profiling, and multiple-azimuth shear-wave experiments have been performed targeting the estimation of in-situ anisotropy (Rabbel et al. 1994; Muller et al, 1999; Okaya et al, 2004; Rabbel et al., 2004). In our experiment, we recover structural information as well as anisotropy of the upper crust using the receiver function technique. This retrieved information is the basis for comparing the outcome from RF analysis in terms of amount and orientation of anisotropy, together with information of rock samples down to 9 km depth, and with high-frequency seismic experiments around the drill (Bianchi et al., 2015a).

2. Anisotropy

Strong seismic anisotropy has been associated to metamorphic processes in several studies (e.g., Christensen, 1965; Barruol and Mainprice, 1993; Christensen and Mooney, 1995; Lloyd et al., 2009; Almqvist and Mainprice, 2017; Okaya et al, 2018). Also, seismic anisotropy has been observed in association to aligned cracks that occur in the vicinity of major faults or due

EAGE Publications B.V., PO Box 59, 3990 DB, Houten, The Netherlands

to upper crustal stress fields (e.g., Anderson et al., 1974; Savage et al., 2010; Almqvist and Mainprice, 2017).

Effects of seismic anisotropy within the crust have been often observed in body and surface waves (e.g., Ozacar and Zandt, 2004; Sherrington et al., 2004; Bostock and Christensen, 2012; Okaya et al., 2016; Bianchi et al., 2016). We want to draw special attention on RF studies, which have observed the pattern of the converted Ps waves for several anisotropic scenarios (e.g. Levin and Park, 1998; Schulte-Pelkum et al., 2005; Eckardt & Rabbel, 2011; Piana Agostinetti et al., 2011; Schulte-Pelkum & Mahan, 2014; Audet, 2015; Bianchi et al., 2015b, and many others).

The location of our seismic experiment has been selected specifically for the presence of the ZEV metamorphic body which has been drilled down to 9 km depth, and investigated both in situ and in laboratory on core samples. The lithological profile of the drilling (Figure 1b) has been subdivided into three main lithological units as follows: a first unit (U1) from 0 to 3.2 km depth consisting of paragneiss containing minor intercalations of amphibolite. A second unit (U2) from 3.2 to 7.3 km depth composed of amphibolite with intercalations of metagabbros, and minor intercalations of gneiss. In the third unit (U3) below 7.3 km depth, the amount of paragneiss prevails as well, reaching the bottom of the drilling hole, at 9.1 km depth (Berckhemer et al., 1997). Anisotropy has been detected as highest in the gneisses (U1 and U3) while the amphibolites and metagabbros (U2) show significant lower anisotropy (Kern et al, 1991); it has been shown on core samples from these units, that the anisotropy reduces drastically for increasing confining pressures (Zang et al., 1996). Laboratory tests on gneiss samples (biotite bearing) from the ZEV, have shown a marked splitting of the shear waves, where the fast wave shows polarization parallel to the foliation, while the slow wave is polarized normal to it (Kern et al, 1991).

EAGE Publications B.V., PO Box 59, 3990 DB, Houten, The Netherlands

Previous investigations in our study location, have shown that the polarization of the fast shear wave is nearly NW-SE down to approximately 4 km depth (i.e. within the shallow gneiss layer), and which is coinciding with the strike direction of the rock foliation (Rabbel, 1994). The information of rock foliation and fractures obtained by the analysis of core samples (Röhr et al., 1990) of the KTB pilot hole (Emmermann, 1989), which reached the depth of about 4 km, were associated to the differential velocity of the fast and slow shear waves detected via vertical seismic profiling in Rabbel (1994). He noticed that the velocity of both P- and fast S-wave diminishes with the decrease of the dip angle of the foliation, while the velocity of the slow S-wave is constant. This is the typical behaviour of the body waves propagating within an hexagonally symmetric medium (e.g. Postma, 1955). Another argument for hexagonal symmetry comes from Stroh et al., (1990), which detected nearly 30% of well-oriented mica (having hexagonal elastic symmetry) in the gneiss units of the ZEV, the amount of anisotropy in the U1 has been estimated to reach 10% (Rabbel, 1994).

Seismic anisotropy has been recognized to be higher at shallow depths (low pressure i.e. up to 200MPa) due to the positive interference of oriented microcracks and texture of the rocks. In particular Kern et al. (1991) finds that microfractures are parallel to the morphological sheet planes in the gneisses extracted from the pilot hole.

Moreover, encountered horizontal stress direction in the borehole are around N150° (Burdy et al., 1997; Plenefisch and Bonjer, 1997), which is not far from the foliation strike and direction of the fast anisotropy; according to Kern et al, 1994, the deviatoric stress field determined at the KTB drilling site might contribute to the seismic anisotropy in situ.

3. Data

We selected good teleseismic events from epicentral distances (Δ) of $30°–100°$ and magnitude $M_b > 5.5$ recorded at two broadband seismic stations deployed for this purpose (see the description of the experiment in Bianchi et al. (2015)).

The amount of collected teleseismic traces allows a reasonable backazimuthal coverage (Figures 2 and 3): events occurred between Δ of 90° and 100° have been included in order to increase the backzimuthal coverage towards the SW direction. The RF data sets were obtained by deconvolution of the vertical from the horizontal recordings into the radial, transverse, and vertical coordinate system, where the radial (R) is computed along the great circle path between the epicenter and the station, positive away from the source, and the transverse (T) direction is calculated 90° clockwise from R. The deconvolution was performed in the frequency domain (Langston, 1979; Ammon et al., 1990; Ammon, 1991), following the approach proposed by Park and Levin (2000), applying a slepian taper to limit the frequency band below about 4 Hz (Langston, 1979). The full data sets were published in Bianchi et al, 2018. Here we use the data from 2 stations deployed by the drilling site, i.e. KW01 and KW06, shown in Figures 2 and 3 as backazimuthal sweeps. The RFs obtained from the teleseismic events have been binned to increase the S/N ratio. Bins are obtained by the stacking of RFs for events occurring in the same backazimuth (+-5deg). The spatial filter used to define the events that belong to a single bin is 20° wide in backazimuth (baz) and 40° wide in Δ. The good backazimuthal coverage makes 3-D structure modelling beneath the two stations possible from both the radial RF (RRF) and transverse RF (TRF) data sets (Figures 2a and 3a).

4. Inversion Method

The 1D shear velocity model beneath the two stations has been investigated by Bianchi & Bokelmann (2018) who generated a-posteriori probability-density function of the v_s at depth following the reversible-jump Markov chain Monte Carlo (rjMcMC) approach developed by Piana Agostinetti and Malinverno (2010). In this paper, we use the recovered isotropic structure as a starting point for constraining a search for 3-D features (i.e. dipping interfaces or/and anisotropic layers), through the neighborhood algorithm (NA) search (Sambridge, 1999). The rjMcMC search yields two main results: the PPD of the *S* velocity at depth, and the distribution of the interface depth sampled during the chain, we used this information to build a parameter space for the following 3-D v_s modeling, and additional information from the TRF component, to give constraints on dipping interfaces and anisotropic layers. The mean v_s model from the rjMcMC search was discretized with reference to the number and depth of the interfaces published in Bianchi & Bokelmann (2018). The v_s models were divided into layers with uniform velocity and anisotropic parameters have been assigned to perform the NA search. According to previous information on the area, we set the possibility to explore the anisotropic parameters within the shallow unit (U1); this main layer is divided into three sublayers. The second layer in our parameter space has been set without anisotropy parameters (this would correspond to the metabasite depth, or the previously defined unit U2). The latter layer (or lower anisotropic layer) has been set with anisotropy, which would correspond to the lower (deeper) gneiss package (U3).

After some initial tentative, we select the parameter space that guarantees the best misfit reduction within a reasonable number of sampled models. To cross-check that our parameter space does not bias our findings, we include in the supplementary material additional results using different parameter spaces. The defined parameter space is shown in Table S1.

Modelling the RF is a classical inverse problem characterized by strong non-uniqueness. Interfaces depths and S-wave velocity, anisotropy percentage and plunge of the anisotropic symmetry axis display a clear trade-off, which makes it difficult to draw simple quantitative inferences from the observations. The stochastic sampling used by the NA algorithm to

EAGE Publications B.V., PO Box 59, 3990 DB, Houten, The Netherlands

explore the multidimensional parameter space for a range of acceptable velocity models uses the properties of Voronoi cells with the aim of finding an ensemble of models with acceptable data fit. We generated 1000 initial random samples inside the parameter space, and the 50 cells with the lowest misfit were resampled to produce 500 new samples. This process was repeated 500 times, for a total of 101,000 models explored for each station. We evaluate the standard deviation of the models parameters on the ensemble of models which generate synthetics that fit the data with 1.10 times lower misfit than the best-fit model. The best fit model is then interpreted as representative of the ensemble. Synthetics are calculated using the RAYSUM code (Frederiksen and Bostock, 2000) that models the propagation of a plane wave in dipping and anisotropic structures. Anisotropy was modeled as hexagonal with a unique axis of symmetry, which fits the characteristics of the transverse isotropy supported by laboratory experiments on the drill core samples (Kern et al., 1991). Here, we do not model multiple phases. To be coherent from many back-azimuthal directions and thus recognizable in the RF patterns, multiple phases need to propagate through a homogeneous (anisotropic) structure covering a circle of about 10-15 km diameter around the station (approximately, for a 5 km depth target). From previous knowledge of the area (as clearly seen in Figure 4a) we understand that the overall structure at the KTB drill site is not horizontally-layered over such scale length; therefore we can assume that the complex local structure prevents multiple phases to be coherently recorded in the RF signal.

4.1 Anisotropy Model

In a hexagonal system, there is a single axis of symmetry; in the plane perpendicular to the axis of symmetry, every direction is indistinguishable. *P*-wave propagation along the axis of symmetry can be either faster or slower than that in the perpendicular plane, corresponding to positive/negative anisotropy (Savage, 1998). We opted for modeling anisotropy with slow symmetry axis due to the previous information on the KTB core samples, where the shear

EAGE Publications B.V., PO Box 59, 3990 DB, Houten, The Netherlands

wave splitting has been recognized as most pronounced in the gneisses which hold a high percentage of mica. The mica as plate-like mineral would have a slow propagation direction parallel to the [001] axis (Alexandrov & Rhyzova, 1961; Kern and Schmidt, 1990), which can be modeled by slow (negative) anisotropy (Levin and Park, 1998). The other factor that may play a role is stress-induced cracks; these would also be characterized by negative anisotropy. Focusing on negative anisotropy alone is not restrictive, since it has already been shown how fast and slow anisotropic axes reproduce the same pattern for opposite trend (e.g. Sherrington et al., 2004, Bianchi et al., 2008; Bianchi et al., 2010). In the considered models, the magnitude (percent) of *P* and *S* anisotropies are set to be equal to reduce the computation time. Dipping interfaces and dipping anisotropic layers produce similar signals that are difficult to distinguish (Savage*,* 1998; Bianchi et al*.*, 2008). Thus, we use the information about the location of anisotropic layers and the amount of anisotropy from previous studies (i.e. Berckhemer et al., 1997) to reproduce 3-D features in the very shallow crust. In our parametrization, a plunge angle of 0° corresponds to a horizontal anisotropy symmetry axis, while a plunge angle of 90° corresponds to a vertical symmetry axis.

5. Results

The output of the inversion method that we have employed here gives us the best-fit model out of a family of models with 31 free parameters inverted. 12 of the 31 free parameters are related to the anisotropic characteristics of the media, and describe trend and plunge of the symmetry axes, as well as the strength of anisotropy (in percent) of the 4 layers (3 sublayers within the U1 + 1 layer in U3) of the velocity model bearing anisotropy.

We therefore focus here on the description of the ~~trend of~~ anisotropy into the two main layers (U1 and U3) in the upper 10 km of the crust. For station KW01, three sublayers of the U1 have anisotropy with a slow axis trending to the SW, for each of these the plunge is less than 25º from the horizontal, and the percentage of anisotropy is increasing from the shallower to the deeper (from 5% to 8%). At 6.5 km depth a deeper anisotropic layer is encountered (U3), which displays a symmetry axis trending to the NE. The counts of single iteration best-fit values for the anisotropic layers (Figure S1) are here shown for the robustness of the results. For station KW06, we run a first search using a 2-layered parameter space with one inclined interface, for constraining the high amplitudes observed within the 1st second of the RFs (Figure 3). The NA search performed returns an interface striking N118 º at 1 km depth beneath the station, which is in agreement with the strike of the faults in the area and mapped by several previous works (e.g. Hirschmann, 1996). Due to the large effect it has on the RF for that station, we have decided to use the subset of data in which the signals from the deeper layers have not been cancelled by the presence of the shallow dipping interface, and that is shown in Figure 3b. Also for this station the NA search finds anisotropy between 2 and 5 km depth, with increasing strength with depth (U1). Yet, the results give a less stable trend of the symmetry axis, probably caused by the imposed restriction of backazimuths and/or by the interference with the encountered dipping interface; at 7.5 km depth the U3 is found, which shows a NE trend of its axis, in agreement with the results for station KW01. Based on the family of the best-fit models (ensemble of models which fit the observed wiggles with a misfit lower than 1.10 times the misfit of the best-fit model) we give estimates on the uncertainties on the inverted parameters (Table 1). Errors on the thickness of the layers vary from ±0.1 km for the shallower layer to ±1.4 km for the lower layer; error on the amount of anisotropy is between ±1 and ±2 %; for the trend of anisotropy we find ±40° error estimate in the first and last layers; this value doubles for the second and third layers, showing the high variability of this result.

To verify that the choice of our parameter space does not bias the solution, we tested the presence of anisotropy in the layer U2. The results converge towards anisotropy with a

EAGE Publications B.V., PO Box 59, 3990 DB, Houten, The Netherlands

nearly vertical axis (plunge equals to 75°+- 8°, Figure S2), thus we exclude the presence of anisotropy there because such a geometry does not generate any relevant signal on the T component of the RF. By enlarging the values of anisotropy magnitude (0 to -15%) and plunge (0° to 90°) for the layers in U1 and U3, we show that the choice of the boundaries of our parameter space does not affect the results of the NA search. In this case, we include models without anisotropy (or with limited effects on T-RF patterns, i.e. plunge angles larger than 60 degrees). The results are shown in Figure S3. Best fit and standard deviation values highlight that a strong anisotropy is still present in layers U1 and U3 (between -5 and -9%), and that the plunge of the symmetry axes are not close to vertical.

6. Discussion

We have determined the anisotropic parameters for a sequence of layers under two seismic stations near the KTB borehole, and we will later compare these in detail with the subsurface structure which is known from the KTB borehole.

Lithological changes with depth, changes in the fabric orientation, presence of zones of mechanical weakness associated with lower seismic velocities as cracks or cataclastic fracture zones, are all factors which contribute to cause anisotropy. We schematize here the main information regarding these points from the wide literature produced by previous studies at the KTB site.

1) The lithological units of the ZEV extend down to the final depth of the borehole and are divided into paragneiss, amphibolites, and variegated (alternating sequences of gneiss and amphibolites) (Figure 1) (Emmermann & Lauterjung,1997). The whole profile can be subdivided into three main uniform units: (U1) consisting of mainly paragneiss (0 to 3.2 km depth), (U2) composed of metabasites, mainly amphibolite, metagabbros and metabasalt (3.2 to 7.3 km depth), and (U3) made of mainly

EAGE Publications B.V., PO Box 59, 3990 DB, Houten, The Netherlands

paragneiss (7.3 km depth until the bottom of the borehole, 9.1 km depth) (Berckhemer et al., 1997).

2) The metamorphic rocks show a steep dip between 60° to 80° towards SW or NE and are strongly folded with subhorizontal axial planes and NNW-SSE trending fold axes (e.g Duyster et al., 1993; Hirschmann and Lapp, 1994). The KTB depth profile has been subdivided into three structural units with homogeneous dip: (U1) mainly SW and minor NE dip, (U2) mainly E and minor W dip, (U3) SW dip (Berckhemer et al., 1999). The local fault system is associated to the Franconian Lineament (FL) which strikes N140° at about 5 km SW from the KTB borehole (Figure 1).

3) The seismic reflectors named SE1 and SE2 are recognized to be cataclastic zones related to the local fault system and related to the FL (Hirschmann, 1992; Hluchy, 1992), outcropping on surface at about 4.5 km distance from KW01. Considering an average dip of 55° to the NE of the faults, we would encounter the SE1 at 6.4 km and at 3.5 km beneath KW01 and KW06 respectively; the estimated depth of SE2 is at about 3.5 km and 2.5 km for stations KW01 and KW06 respectively. These two also largely correspond to the boundaries between the three lithologically uniform units below station KW01.

4) Stress measurements in the pilot hole (Baumgärtner et al, 1990; Mastin et al., 1991) show a NNW-SSE oriented direction of maximum horizontal principal stress and strike-slip to normal faulting stress magnitudes. The wave velocities at the KTB drill site are affected by the presence of open microcracks until a critical depth of 5-6 km (Kern et al., 1991); according to the same author, in the mica-rich genisses the oriented microfractures are occurring parallel to the morphological sheet planes.

5) A fast anisotropic axis (for both compressional and shear waves) has been detected oriented NW-SE parallel to the foliation planes of the metamorphic body (Rabbel,

1994, Berckhemer et al., 1997; Harjes et al., 1997). Based on array data in a similar setting (GERESS array), Bokelmann (1995) had also found a good agreement of the orientation of fast planes with the known foliation orientation of rocks in the area (based on P-wave polarization). Laboratory measurements on rock samples had predicted a considerable amount of anisotropy (Stroh et al.,1990; Kern et al.,1991; Siegesmund et al.,1993). Lüschen et al. (1991,1996) and Rabbel (1994) proved the existence of split shear waves with an observed velocity difference of up to 10%, locally even as high as 14% (Rabbel, et al., 2004).

To compare with rock fabrics, we inspect the retrieved trend and plunge angles of the slow anisotropic axes, and project them on the SW-NE cross section of the ZEV summarizing the main orientation of the foliation and of the faults (Hirschmann, 1996) (Figure 4a). For the deeper anisotropic layer found at both stations, the inferred NE-trend of the slow anisotropic axis corresponds to the minimum velocity of the seismic wave, which is perpendicular to the rock foliation in mica-rich rocks such as the gneiss of the ZEV. We know from literature that the foliation planes are dipping to the SW; that would therefore fit to a symmetry axis of the mica plunging towards the NE. We observe therefore a perfect fit between the true foliation dipping to SW (shown in the background of Figure 4a), and the foliation obtained by the inferred anisotropy symmetry axis (blue lines, Figure 4a), we therefore attribute the anisotropy as caused by textural velocity. The inferred NE-trend of the slow axis is also perpendicular to the NW-SE fast anisotropy axis from previous studies (e.g. Bopp, 1992; Rabbel, 1994; Rabbel et al., 2004). In the shallower layer we may also be dealing with open cracks that would be expected to be aligned with the stress field up to several kilometers depth (Kern et al., 1991), we know that the tectonic stress in the vicinity of the KTB is expected to have an orientation of (N150°E) (Zoback et al., 1993). All three factors potentially causing seismic anisotropy (fabric, faults and σ_H-aligned cracks) are striking in NW-SE

EAGE Publications B.V., PO Box 59, 3990 DB, Houten, The Netherlands

orientation, but faulting and foliation dip towards opposite directions and affecting the wave propagation; we argue that the causes of the deviation from being parallel to the texture are due to the combined influence of faults and cracks.

The striking finding of our analysis is the perfect match between the depth and thickness of the mica-rich gneiss found in the core-log and the depth extent of the inferred anisotropic U1 and U3 layers. Figure 4a shows that RF data constrain anisotropy within the gneiss layers, avoiding the amphibolite layer even if the parameter space (Table S1) gives a potential thickness for U1 between 1 and 5 km, and a potential boundary between U2 and U3 between 2 and 8 km. Locating anisotropy at depth is a difficult task for exploration geophysics (e.g. repeated AVO is a common but expensive tool (Rüger, 2001)). It is of particular interest that we can demonstrate here a relatively cheap method able to locate the anisotropic rock volumes at depth. Accounting for anisotropy has strong implication for reservoir characterization, since its presence might cause significant problems in the interpretation of active seismic data and therefore on the properties of investigated depth structures (e.g. Asaka, 2018). We have seen that receiver functions can provide important information on the subsurface location and character of seismic anisotropy from passively-recorded data. The application is computationally efficient, and it may in principle be of interest also for industrial (e.g. oil/gas) applications, as well as underground storage, although it will in general not yield a resolution comparable with that of reflection data (e.g., Tsvankin et al., 2010), due to the longer wavelengths.

7. Conclusions

With the application of the receiver function, a passive seismological technique, in the KTB area in Southern Germany, we have acquired some unique proof of the direct correspondence between in-situ rock texture and seismic anisotropy.

EAGE Publications B.V., PO Box 59, 3990 DB, Houten, The Netherlands

We gain information below two seismic stations located nearby the KTB drilling hole, where we verify the presence of in situ anisotropy, in particular, we infer the presence of two distinct anisotropic layers within the upper crust. The depth of these two layers corresponds to the location of mica-rich paragneiss which show intense foliation, this let us gain larger information with respect to previous in situ studies where anisotropy was identified as due to the entire ZEV thickness. We infer higher anisotropic percentages at shallower depths probably related to the presence of cracks. Concerning the causes of the seismic anisotropy we conclude that for the lower anisotropic layer the symmetry axis of the slow shear-wave is perpendicular to the main foliation of the paragneiss, and is ascribed as due to the alignment of the minerals (micas), while for the upper anisotropic layer, the slow anisotropic axis deviates from being perpendicular to the foliation plane, probably due to the presence of intense faulting and of the crack system. Moreover, RF can provide important information on the depth location of seismic anisotropy, and can be used as a complementary or explorative tool for underground exploitation, due to its computational efficiency and low cost.

Acknowledgements: We thank Hans-Albert Dahlheim for his precious advice, and help during the field campaign. We are also grateful to Franz Holzförster, scientific director of the KTB Geozentrum, for giving us the opportunity to use the spaces of the geo-center. We thank Wolfgang Rabbel for helpful discussion. We acknowledge funding by the Austrian Science Fund (FWF): 24218. We thank T. Taymaz and two anonymous reviewers for the constructive comments on the manuscript.

Expects Data: Data used for this study are stored at the Department of Meteorology and Geophysics of the University of of Vienna, for access please email to irene.bianchi@univie.ac.at.

Figure Captions

Figure 1:

a) Map of the KTB area showing the location of the two main stations analysed in this work with respect to the location of the KTB drilling site. (R3) b) Schematization of the lithological profile encountered during drilling, and Vp velocity extracted from the sonic log, (both from Berckhemer et al., 1997)

Figure 2:

Comparison between observed (left) and synthetic (right) receiver functions calculated for station KW01. Synthetics have been computed for the model shown in Table 1. Blue arrows on the T component show the pulses associated with anisotropy.

Figure 3:

Comparison between observed (left) and synthetic (right) receiver functions calculated for station KW06. Upper panels show the whole backazimuthal sweep, lower panels show the selected backazimuthal directions. Synthetics have been computed for the model shown in Table 2. Yellow arrow show the pulse associated to a shallow dipping interface, blue arrows show the pulses associated with anisotropy.

Figure 4:

a) In the background a schematic representation of the ZEV metamorphic body showing the location and depth of the drilling site with respect to the reconstructed structures of the metamorphic rocks (modified after Hirschmann, 1996). Double-sided arrows show the orientations of slow anisotropic axes projected along a SW-NE profile cutting the ZEV metamorphic body. Blue lines are drawn normal to the slow axes. The orientation of the blue lines is subparallel to the foliation planes for the lower layer and for the upper layer below KW06, while it deviates for the upper layer below station KW01. Note the remarkable agreement of the inferred orientation of the foliation (blue lines) with geological features. b) S-wave velocity-depth profile (black dashed line) for station KW01, blue area shows the depth location of anisotropic layers, gray dashed lines show the amount of anisotropy in each layer, plunge and trend angles of the anisotropy axes are specified; c) same as b for station KW06, blue dashed line shows the location of the inclined interface.

Figure S1:

Count of single-iteration best-fit values for anisotropy concerning anisotropy strength, trend (from N) and plunge (from horizontal) (respectively upper, middle and bottom row), for the four anisotropic layers modelled for station KW01.

Figure S2: Count of single-iteration best-fit values for anisotropy concerning anisotropy strength, trend (from N) and plunge (from horizontal) for the layer U2, black dashed line shows the value of the best-fit model, and grey dashed lines show the standard deviation.

Figure S3: Count of single-iteration best-fit values for anisotropy concerning anisotropy strength, and plunge (from horizontal) for the layers in U1 and U3 considering an unconstrained parameter space. Black dashed line shows the value of the best-fit model, and grey dashed lines show the standard deviation, these values are also reported in each panel.

Figure S4: a and b) Map view showing the trend of anisotropic axes (in a the upper layer, and in b the lower layer) in relation with the maximum horizontal stress (σ_H) and the surface trace of the FL.

Table 1: velocity model for KW01

		Thickness (km)	v_s (km/s)	v_p/v_s	P-S wave anisotropy (%)	Trend	Plunge	Strike	Dip
U1	**sublay1**	0.9±0.1	2.4	1.77	-5±1	250±40	24±5		
	sublay2	1.8±0.3	3.3	1.76	-7±2	240±80	6±3		
	sublay3	1.2±0.3	3.6	1.71	-8±2	250±70	17±5		
U2		2.3±0.4	3.3	1.73					
U3		7±1	3.6	1.72	-5±1	15±40	26±5		
		halfspace	3.8	1.71				60	40

Table 2: velocity model for KW06

		Thickness (km)	v_s (km/s)	v_p/v_s	P-S wave anisotropy (%)	Trend	Plunge	Strike	Dip
		1	1.4	1.63					
		1	1.9	1.73				118	24
U1	**sublay1**	0.5±0.4	2.9	1.79	-9±3	50±90	40±10		
	sublay2	1.8±0.2	3.6	1.73	-13±3	350±90	20±10		
	sublay3	0.5±0.4	3.8	1.75	-15±3	250±90	0±10		
U2		2.8±0.5	3.3	1.70					
U3		4.5±0.5	3.5	1.73	-7±2	40±70	60±10		
		halfspace	3.7	1.76				314	30

REFERENCES

Alexandrov, K. S., Rhyzova, T. J. 1961. Elastic properties of the rock-forming minerals: layered silicates. Izv. Geophys. Ser. 1961, 1799–1804.

Almqvist, B.S.G., and Mainprice, D. 2017. Seismic properties and anisotropy of the continental crust: Predictions based on mineral texture and rock microstructure: Reviews of Geophysics, v. 55, p. 367–433, https://doi.org/10.1002/2016RG000552

Ammon, C.J. 1991. The isolation of receiver effects from teleseismic P waveforms, Bull. seism. Soc. Am.,81(6), 2504–2510.

Ammon, C.J., Randall, G.E. & Zandt, G. 1990. On the non-uniqueness of receiver function inversions, J. geophys. Res.,95(B10), 15 303–15 318

Anderson, D.L., Minster, B., and Cole, N. 1974. The effect of oriented cracks on seismic velocities: Journal of Geophysical Research, v. 79, p. 4011–4015, https://doi.org/10.1029/JB079i026p04011.

Asaka, M. 2018. Anisotropic AVO: Implications for reservoir characterization The Leading Edge 2018 37:12, 916-923

Audet, P. 2015. Layered crustal anisotropy around the San Andreas Fault near Parkfield, California, J. Geophys. Res. Solid Earth, 120, 3527–3543, doi:10.1002/2014JB011821.

Babuška, V., Cara, M. 1991. Seismic Anisotropy in the Earth. Kluwer Academic Publishers, London.

Barruol, G., and Mainprice, D. 1993. 3-D seismic velocities calculated from lattice-preferred orientation and reflectivity of a lower crustal section: examples of the Val Sesia section (Ivrea zone, northern Italy: Geophysical Journal International, v. 115, p. 1169–1188, https://doi.org/10.1111/j.1365-246X.1993.tb01519.x.

Baumgartner, J., Rummel, F. and Zoback M. D. 1990. Hydraulic fracturing in situ stress measurements to 3 km depth in the KTB pilot hole VB, KTB Rep 90-6a, pp. 353-399, Niedersächsisches Landesamt Rir Bodenforsch., Hannover, Germany.

Bopp, M. 1992. Shear-wave splitting observed by wide-angle measurement. KTB Report, 92-5:297-308.

Berckhemer, H., Rauen, A., Winter, H., Kern, H., Kontny, A., Lienert, M., Nover, G., Pohl, J., Popp, T., Schult, A., Zinke, J., Soffel, H.C. 1997. Petrophysical properties of the 9-km-deep crustal section at KTB. J. Geophys. Res. 102, 18,337 – 18,361.

Bianchi, I., Piana Agostinetti, N., De Gori, P., Chiarabba C. 2008. Deep structure of the Colli Albani Volcanic District (central Italy) from Receiver Function analysis. J. Geophys. Res., 113, B09313, doi:10.1029/2007JB005548.

Bianchi, I., Park, J., Piana Agostinetti, N., Levin V. 2010. Mapping seismic anisotropy using harmonic decomposition of Receiver Functions: an application to Northern Apennines, Italy. J. Geophys. Res.,115, B12317, doi:10.1029/2009JB007061.

Bianchi, I., Anselmi, M., Apoloner, M.T., Qorbani, E., Gribovski, K. & Bokelmann, G. 2015a. The installation campaign of 9 seismic stations around the KTB site to test anisotropy detection by the Receiver Function Technique, Adv. Geosci.,41,11–23

Bianchi, I., Bokelmann, G., Shiomi, K. 2015b. Crustal anisotropy across northern Japan from receiver functions, Journal of Geophysical Research: Solid Earth, 120/7, DOI: 10.1002/2014JB011681

Bianchi, I., Lucente, F. P., Di Bona, M., Govoni, A., Piana Agostinetti, N. 2016. Crustal structure and deformation across a mature slab tear zone: the case of southern Tyrrhenian Subduction (Italy), Geophys. Res. Lett; 10.1002/2016GL070978, accepted for publication

Bianchi, I., Bokelmann, G. 2018. Imaging the Variscan suture at the KTB deep drilling site, Germany, Geophysical Journal International, 213, 3, 1, 2138–2146, doi.org/10.1093/gji/ggy098

Bostock, M.G., and Christensen, N.I. 2012. Split from slip and schist: crustal anisotropy beneath northern Cascadia from non-volcanic tremor: Journal of Geophysical Research, v. 117, B08303, https://doi.org/10.1029/2011JB009095.

Bokelmann, G.H.R. 1995. P-wave array polarization analysis and effective anisotropy of the brittle crust, Geophys. J. Int., 120, 145-162

Brudy, M., Zoback, M. D., Fuchs, F., Rummel, F. & Baumgärtner, J. 1997. Estimation of the complete stress tensor to 8 km depth in the KTB scientific drill holes: implications for crustal strength. Journalof GeophysicalResearch, 102(B8), 18453-18457

EAGE Publications B.V., PO Box 59, 3990 DB, Houten, The Netherlands

Christensen, N.I. 1965. Measurements of dynamic properties of rock at elevated temperatures and pressures, *in* Pincus, H.J., and Hoskins, E.R., eds., Measurements of Rock Properties at Elevated Pressures and Temperatures: Philadelphia, American Society for Testing Materials STP869, p. 93–107.

Christensen, N.I., and Mooney, W.D. 1995. Seismic velocity structure and composition of the continental crust: A global review: Journal of Geophysical Research, v. 100, p. 9761–9788, https://doi.org/10.1029/95JB00259.

DEKORP Research Group 1987. Near-vertical and wide-angle seismic surveys in the Black Forest, SW Germany, J. Geophys.,62,1–30.

DEKORP Research Group 1988. Results of the DEKORP 4/KTB Oberpfalz deep seismic reflection investigations, J. Geophys.,62,69–101.

DEKORP and Orogenic processes Working Groups 1999. Exhumation of subducted crust—the Saxonian granulites from reflection seismic experiment GRANU' 95, Tectonics, 18, 756–773

Duyster, J., Kontny, A., deWall, H., Zulauf G. 1995. Postvariszische Krustenstapelung am Westrand der Böhmischen Masse, Geowissenschaften, 134, 135–141.

Eckhardt, C., Rabbel W. 2011. *P*-receiver functions of anisotropic continental crust: a hierarchic catalogue of crustal models and azimuthal waveform patterns, *Geophysical Journal International*, 187, 1, 439–479, https://doi.org/10.1111/j.1365-246X.2011.05159.x

Girardin, N., and Farra, V. 1998. Azimuthal anisotropy in the upper mantle from observation of P-to-S converted phases: Application to southeast Australia, Geophys. J. Int., 133, 615–629.

Frederiksen, A.W., & Bostock, M.G. 2000. Modelling teleseismic waves in dipping anisotropic structures, Geophys. J. Int.,141(2), 401–412.

Eisbacher, G.-H., Lueschen, E. & Wickert, F. 1989. Crustal-scale thrusting and extension in the Hercynian Schwarzwald and Vosges, Central Europe,Tectonics,8(1), 1–21.

Emmermann, R. 1989. The KTB pilot hole: tectonic setting, technical data and first results, in The German Continental Deep Drilling Program(KTB): Site-selection Studies in the Oberpfalz and Schwarzwald, pp. 527–553, eds Emmermann, R. & Wohlenberg, J., Springer Verlag.

Haak, V. & Jones, A. 1997. Introduction to special section: the KTB deep drill hole, J. geophys. Res.,102(18), 175–177.

Harjes, H.P. et al. 1997. Origin and nature of crustal reflections: results from integrated seismic measurements at the KTB superdeep drilling site, J. geophys. Res.,102(B8), 18 267–18 288.

Hirschmann, G., Lapp *M.* 1995. Evaluation of the structural geology of the KTB Hauptbohrung (KTB-Oberpfalz HB) *KTB Rep. 94-1,* 285–308 *Niedersächsisches Landesamt für Bodenforsch.,* Hannover, Germany.

EAGE Publications B.V., PO Box 59, 3990 DB, Houten, The Netherlands

Hirschmann, G., 1996. KTB—the structure of a Variscan terrane boundary: seismic investigation—drilling—models, Tectonophysics,264,327–339.

Hluchy, P., M. Körbe, R. Thomas 1992. Preliminary interpretation of the 3D-seismics survey at the KTB location*KTB Rep. 92-5,* 31–52*Niedersächsisches Landesamt für Bodenforsch.,* Hannover, Germany.

Kern H. and Schmidt, R. 1990. Physical Properties of KTB Core Samples at Simulated In-situ Conditions, *Scientific Drilling.* **1**, 217–223.

Kern H., Schmidt, R. and Popp, T. 1991. The Velocity and Density Structure of the 4000m Crustal Segment at the KTB Drilling Site and their Relationship to Lithological and Microstructural Characteristics of the Rocks: an Experimental Approach, *Scientific Drilling* **2**, 130–145.

Kern, H., Popp, T. & Schmidt, R. 1994. The effect of a deviatoric stress on physical rock properties. Surv Geophys 15: 467

Langston, C.A., 1979. Structure under Mount Rainier, Washington, inferred from teleseismic body waves, J. geophys. Res.,84(B9), 4749–4762.

Lüschen, E., Soellner, W., Hohrath, A., Rabbel *W.* 1991. Integrated P- and S-wave borehole experiments at the KTB deep drilling site in the Oberpfalz area (SE Germany), Continental Lithosphere: Deep Seismic Reflections, Geodyn. Ser., 22R. Meissner, *et al.,* 121–133, *AGU,* Washington, D.C.

Lüschen, E., Bram, K., Söllner, W. & Sobolev, S., 1996. Nature of seismic reflections and velocities from VSP-experiments and borehole measurements at the KTB deep drilling site in southeast Germany, Tectonophysics, 264, 309–326.

Levin, V., and JPark J., 1998. P-SH conversions in layered media with hexagonally symmetric anisotropy: A cookbook, Pure Appl. Geophys., 151(2–4), 669–697.

Licciardi, A., Eken, T., Taymaz, T., Agostinetti, N. P., & Yolsal-Çevikbilen, S. 2018. Seismic anisotropy in central North Anatolian Fault Zone and its implications on crustal deformation. Physics of the Earth and Planetary Interiors, 277, 99-112.

Lloyd, G. E., Butler, R. W., Casey, M., & Mainprice, D. 2009. Mica, deformation fabrics and the seismic properties of the continental crust. Earth and Planetary Science Letters, 288(1-2), 320-328.

Mastin, L.G., Heinemann, B., Krammer, A., Fuchs, K. & Zoback, M.D. 1991. Stress orientation in the KTB pilot hole determined from wellbore breakouts, Sci. Drill., 2, 1-12.

Muller, J., Janik, M., & Harjes, H.-P. 1999. The use of wave-field directivity for velocity estimation: moving source profiling (MSP) experiments at KTB, Pure appl. Geophys.,156(1/2), 303–318.

O'Brien, P. J., Duyster J., Grauert B., Schreyer W., Stoeckhert W., and Weber, K. 1997. Crustal evolution of the KTB drill site: From old-est relics to the late Hercynian granites, J. Geophys. Res.-Sol.Ea., 102, 18203–18220.

EAGE Publications B.V., PO Box 59, 3990 DB, Houten, The Netherlands

Okaya, D., Rabbel, W., Beilecke, T., Hasenclever, J. 2004. P wave material anisotropy of tectono-metaorphic terrane: an active source seismic experiment at the KTB super-deep drill hole, southeast Germany. Geophys. Res. Lett. 31, L24620. doi:10.1029/2004GL020855.

Okaya, D., Christensen, N.I., Ross, Z., and Wu, F. 2016. Terrane-controlled crustal shear wave splitting in Taiwan: Geophysical Research Letters, v. 43, p. 556–563, https://doi.org/ 10.1002/2015GL066446.

Okaya, D., Vel, S.S., Song, W.J., and Johnson, S.E. 2019. Modification of crustal seismic anisotropy by geological structures (“structural geometric anisotropy”): Geosphere, v. 15, no. 1, p. 146– 170, https://doi.org/10.1130/GES01655.1.

Ozacar, A., and Zandt, G., 2004. Crustal seismic anisotropy in central Tibet: implications for deformational style and flow in the crust: Geophysical Research Letters, v. 31, L23601, https://doi.org/10.1029/2004GL021096.

Park, J. & Levin, V., 2000. Receiver functions from multiple-taper spectral correlation estimates, Bull. seism. Soc. Am,90,1507–1520.

Piana Agostinetti, N., I. Bianchi, A. Amato, A., Chiarabba C. 2011. Fluid Migration in Continental Subduction. Earth Planet. Sci. Lett., 302, 3-4, 267-278. ISSN 0012-821X, http://dx.doi.org/10.1016/j.epsl.2010.10.039

Piana Agostinetti, N., & Malinverno, A., 2010. Receiver function inversion by trans-dimensional Monte Carlo sampling, Geophys. J. Int., 181, 858–872

EAGE Publications B.V., PO Box 59, 3990 DB, Houten, The Netherlands

Postma, G. W., 1955, Wave propagation in a stratified medium: Geophysics, Soc. of Expl. Geophys., 20,780-806

Plenefisch, T., Bonjer, K.P., 1997. The stress field in the Rhine Graben area inferred from earthquake focal mechanisms and estimation of frictional parameters. Tectonophysics 275, 7–97.

Rabbel, W., Beilecke, T., Bohlen, T., Fischer, D., Frank, A., Hasenclever, J., Borm, G., Kück, J., Bram, K., Druivenga, G., Lüschen, E., Gebrande, H., Pujol, J., Smithson, S. 2004. Superdeep vertical seismic profiling at the KTB deep drill hole (Germany): seismic close-up view of a major thrust zone down to 8.5 km depth. J. Geophys. Res. 109, B09309

Rüger, A., 2001, Reflection coefficients and azimuthal AVO analysis in anisotropic media, Geophysical Monograph Series, 10, ISBN 1-56080-107-7

Sambridge, M. 1999. Geophysical inversion with a neighbourhood algorithm—I. Searching a parameter space, Geophys. J. Int., 138, 479–494.

Savage, M. K. 1998. Lower crustal anisotropy or dipping boundaries? Effects on receiver functions and a case study in New Zealand, *J. Geophys. Res.*, 103(B7), 15069– 15087, doi:10.1029/98JB00795.

Savage, M.K., Wessel, A., Teanby, N.A., and Hurst, A.W. 2010. Automatic measurement of shear wave splitting and applications to time varying anisotropy at Mt. Ruapehu volcano, New Zealand: Journal of Geophysical Research, v. 115, B12321, https://doi.org/ 10.1029/2010JB007722.

Schulte-Pelkum, V., Monsalve, G., Sheehan, A., Pandey, M. R., Sapkota, S., Bilham, R., & Wu, F. 2005. Imaging the Indian subcontinent beneath the Himalaya. Nature, 435(7046), 1222.

Schulte-Pelkum, V. and Mahan, K.H., 2014. A method for mapping crustal deformation and anisotropy with receiver functions and first results from USArray, Earth Planet planet. Sci. Lett., 402, 221–233.

Sherrington, H. F., Zandt, G., and Frederiksen, A. 2004. Crustal fabric in the Tibetan Plateau based on waveform inversions for seismic anisotropy parameters, J. Geophys. Res.,109, B02312, doi:10.1029/2002JB002345.

Siegesmund, S., Vollbrecht, A., Chlupac, T., Nover, G., Dürrast, H., Müller, J. Weber, K. 1993. Fabric-controlled anisotropy of petrophysical properties observed in KTB core samples, Sci. Drill., 4, 31–54.

Stroh, A., Hansmann, J., Heinschild, H. J., Homann, K. D., Tapfer, M., Wittenbecker, M., and Zimmer, M., 1990. Drill hole KTB Oberpfalz VB, Geoscientific investigations in the KTB-field laboratory, depth interval 0-4000.1 m, Geochemistry/mineralogy. KTB-Rep.,90-8:C1-C37.

Tsvankin, I., J. Gaiser, V. Grechka, M. van der Baan, and L. Thomsen, 2010, Seismic anisotropy in exploration and reservoir characterization: An overview, Geophysics, 75, 5, 75A15–75A29, doi:10.1190/1.3481775

Zang, A., Lienert, M., Zinke, J., Berckhemer H. 1996. Residual strain, wave speed and crack analysis of crystalline cores from the KTB-VB well, Tectonophysics, 263, 1–4, 219-234, https://doi.org/10.1016/S0040-1951(96)00033-9.

Zoback, M. D., Apel, R., Baumgärtner, J., Burdy, M., Emmermann R., Engeser, B., Fuchs, K., Kessels, W., Rischmüller, H., Rummel, F., Vernik, L. 1993. Upper-crustal strength inferred from stress measurements to 6 km depth in the KTB borehole, Nature, 365, 633-635.

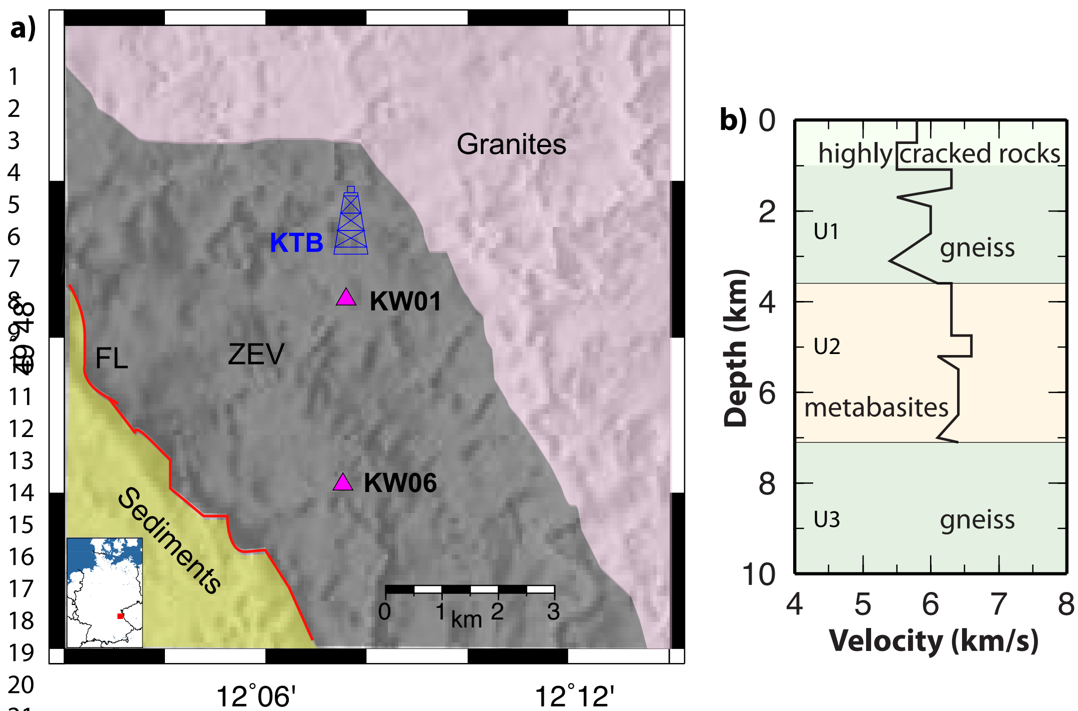
a)
Granites
KTB
KW01
FL
ZEV
KW06
Sediments
0
1
km
2
3
12˚06'
12˚12'
b)
highly cracked rocks
U1
gneiss
U2
metabasites
U3
gneiss
Depth (km)
0
2
4
6
8
10
4
5
6
7
8
Velocity (km/s)

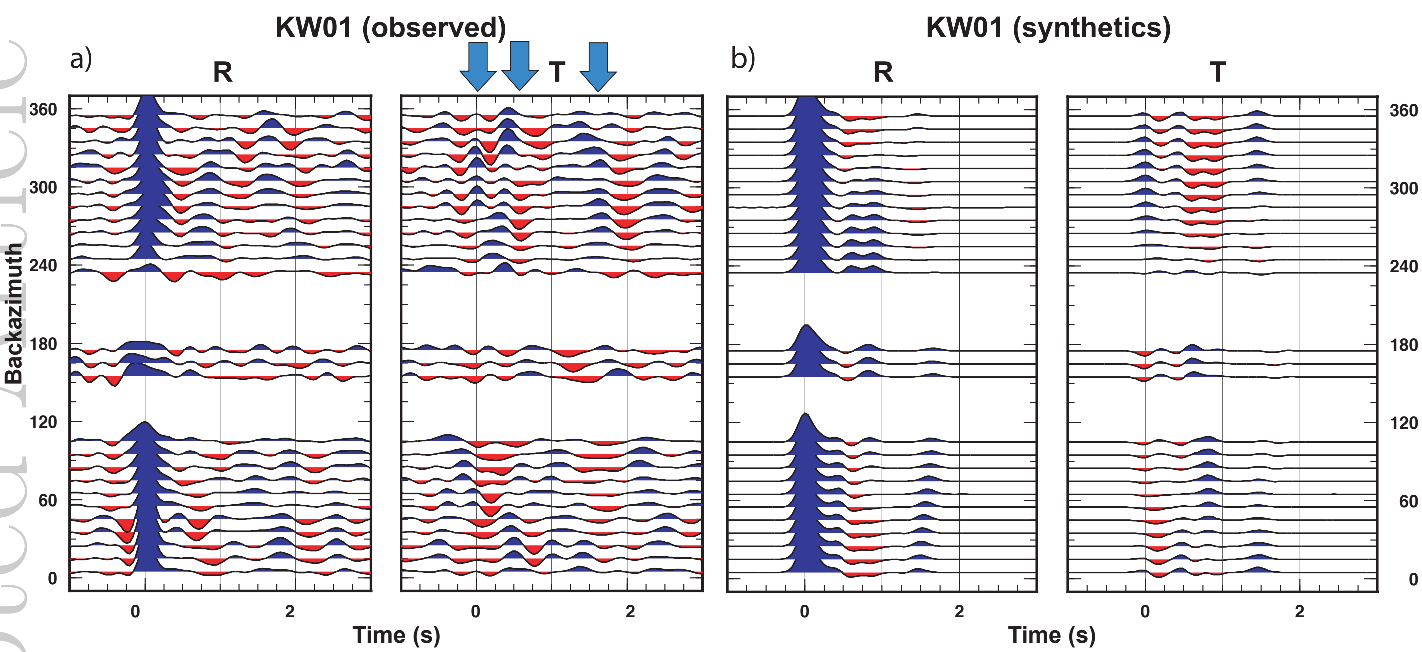
KW01 (observed)
KW01 (synthetics)
a)
b)
R
T
R
T
Backazimuth
360
300
240
180
120
60
0
0
2
Time (s)

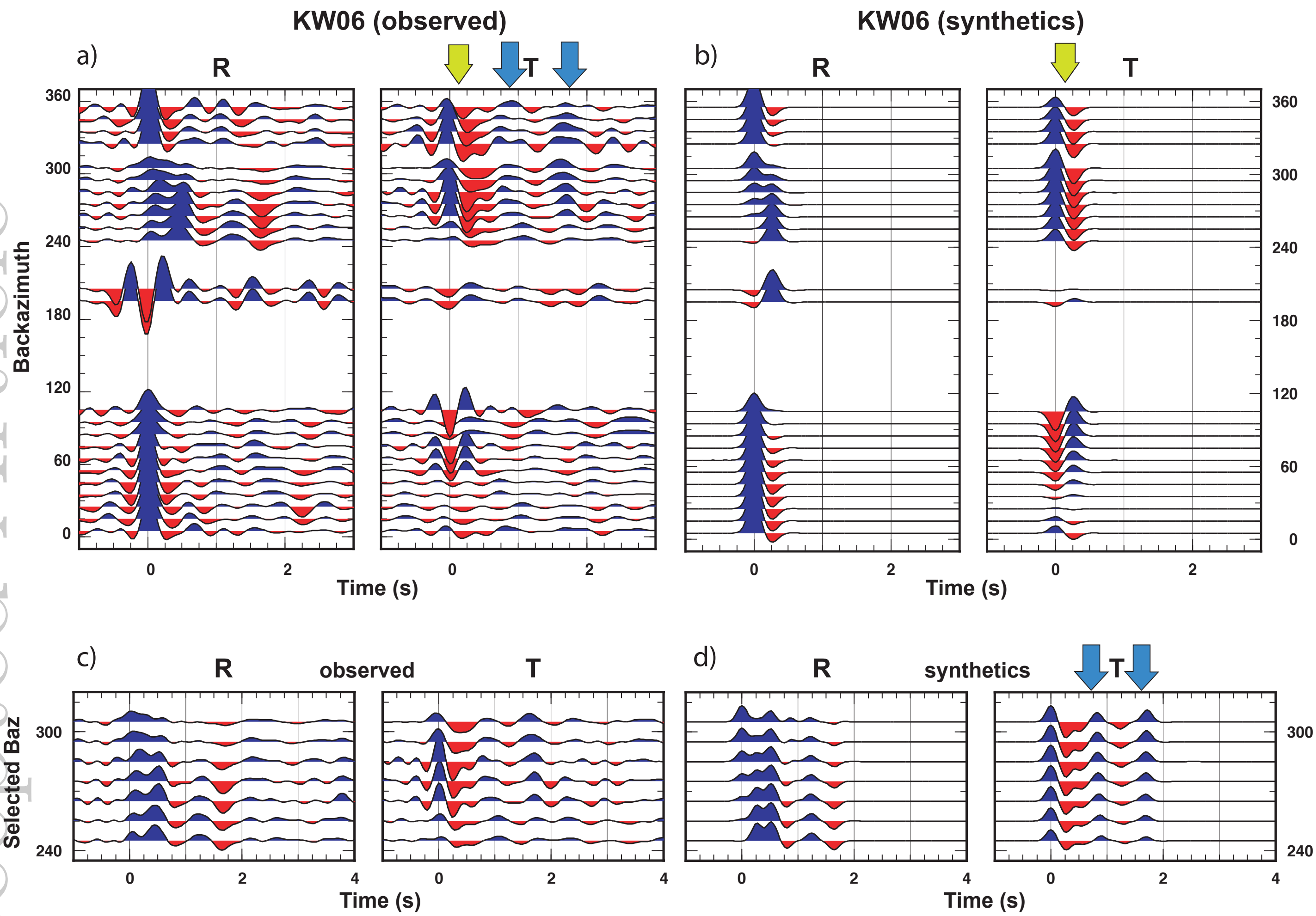

KW06 (observed)
KW06 (synthetics)
a)
R
T
b)
R
T
360
300
240
180
120
60
0
Backazimuth
0
2
Time (s)
c)
R
observed
T
d)
R
synthetics
T
300
240
Selected Baz
0
2
4
Time (s)

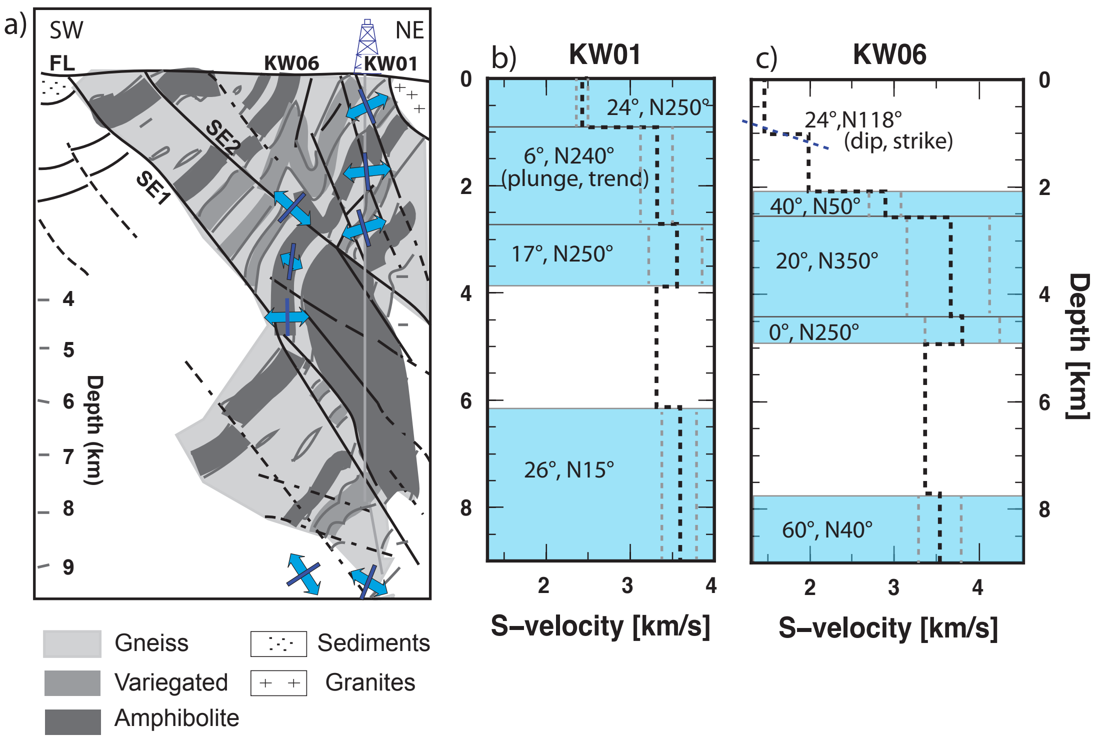
a)
SW
NE
FL
KW06
KW01
SE2
SE1
4
5
6
7
8
9
Depth (km)
Gneiss
Variegated
Amphibolite
Sediments
Granites
b)
KW01
0
2
4
6
8
24°, N250°
6°, N240°
(plunge, trend)
17°, N250°
26°, N15°
2
3
4
S−velocity [km/s]
c)
KW06
24°,N118°
(dip, strike)
40°, N50°
20°, N350°
0°, N250°
60°, N40°
2
3
4
S−velocity [km/s]
Depth [km]

KW01							
Thickness (km)	Vs (km/s)	Vp/Vs	P-S wave anisotropy (%)	Trend	Plunge	Strike	Dip
0.2/1.0	2/3	1.70/1.79	-5/-15	0/360	20/60		
0.5/2.0	3.3/3.8	1.70/1.79	-5/-15	0/360	0/60		
0.3/2.0	3.5/3.8	1.70/1.79	-5/-15	0/360	0/60		
1.0/3.0	3.3/3.8	1.70/1.79					
2.0/8.0	3.5/3.8	1.70/1.79	-5/-15	0/360	20/60		
halfspace	3.7/4.0	1.70/1.79				0/360	30/70
KW06							
1	1.4	1.63					
0.5/2.5	2.0	1.73				118	24
0.2/1.0	2/3	1.70/1.79	-5/-15	0/360	20/60		
0.5/2.0	3.3/3.8	1.70/1.79	-5/-15	0/360	0/60		
0.3/2.0	3.5/3.8	1.70/1.79	-5/-15	0/360	0/60		
1.0/3.0	3.3/3.8	1.70/1.79					
2.0/8.0	3.5/3.8	1.70/1.79	-5/-15	0/360	20/60		
halfspace	3.7/4.0	1.70/1.79				0/360	30/70

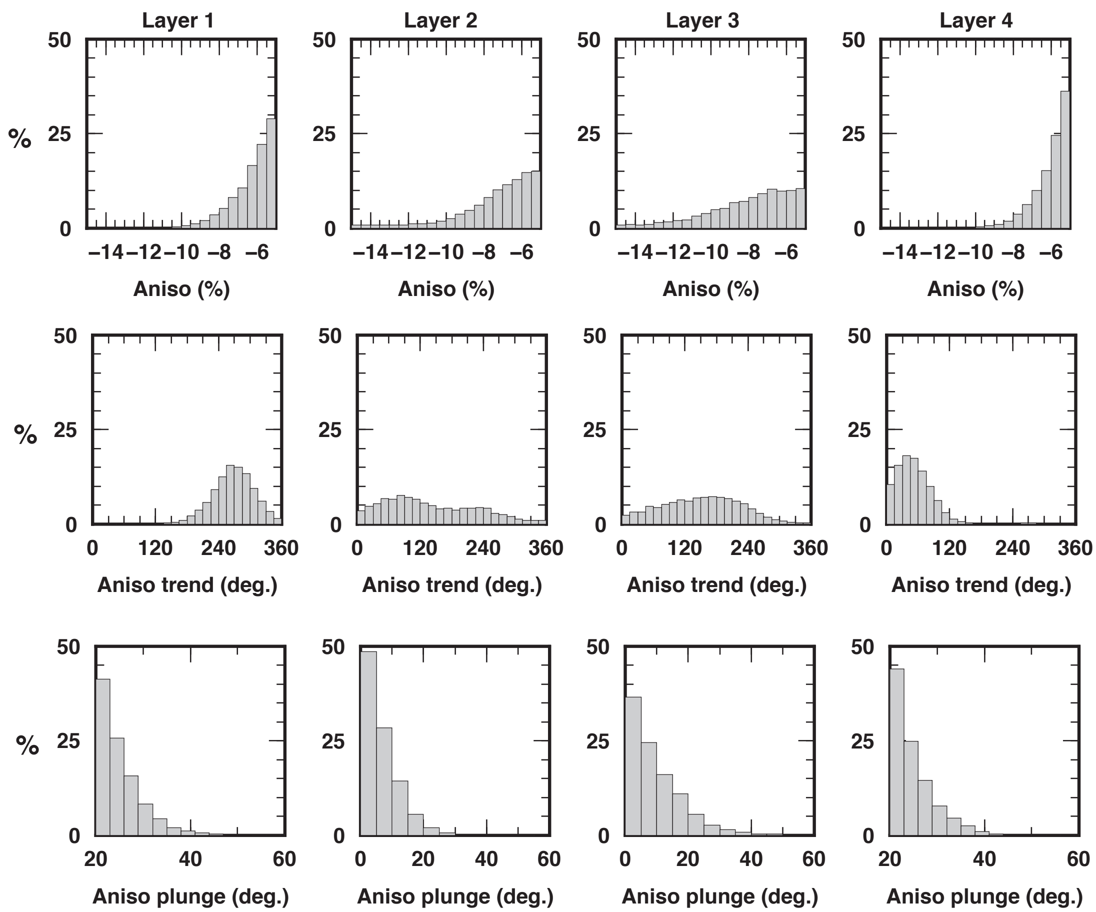
Layer 1
Layer 2
Layer 3
Layer 4
%
50
25
0
–14 –12 –10 –8 –6
Aniso (%)
0
120
240
360
Aniso trend (deg.)
20
40
60
Aniso plunge (deg.)

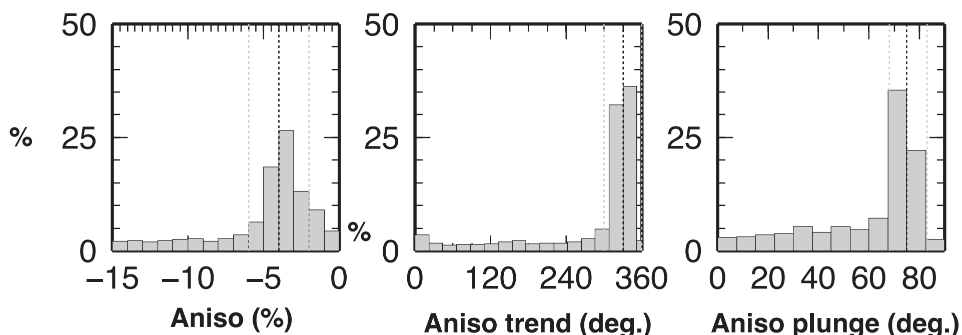

EAGE Publications B.V., PO Box 59, 3990 DB, Houten, The Netherlands

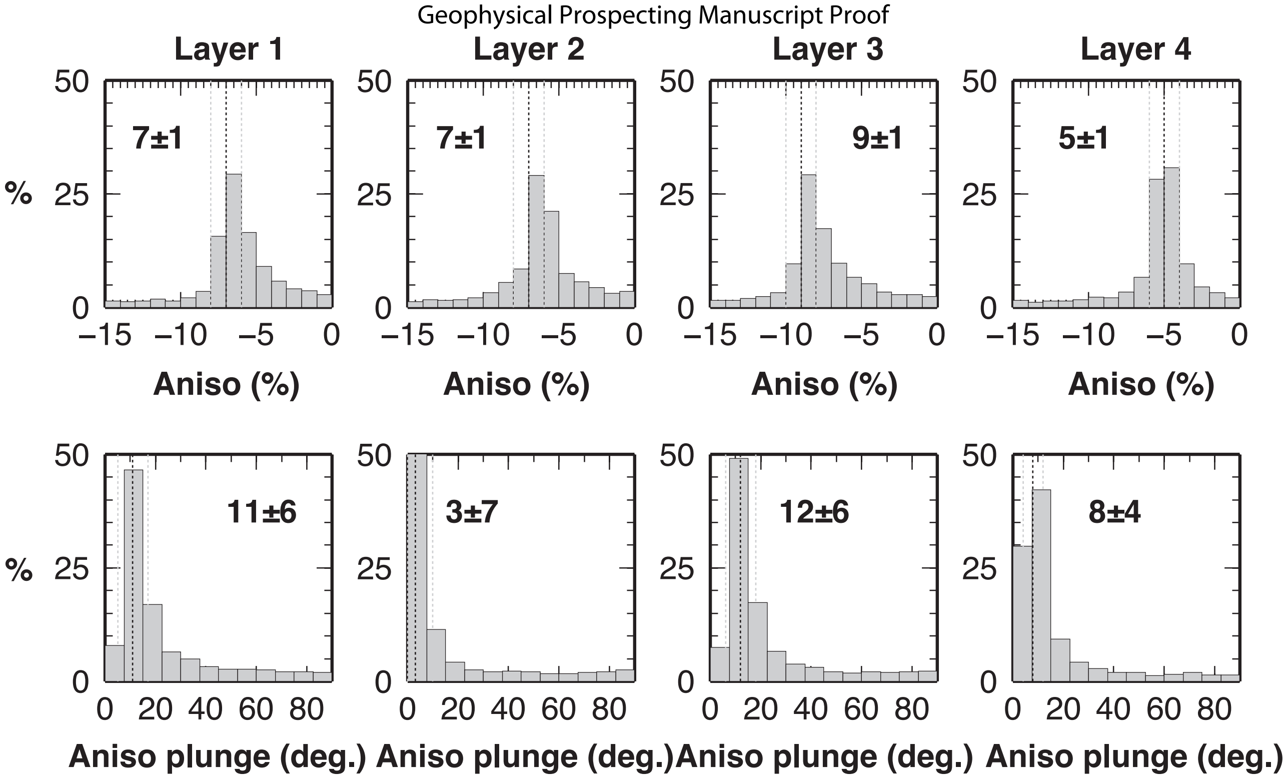

Layer 1
Layer 2
Layer 3
Layer 4
7±1
7±1
9±1
5±1
%
Aniso (%)
11±6
3±7
12±6
8±4
Aniso plunge (deg.)

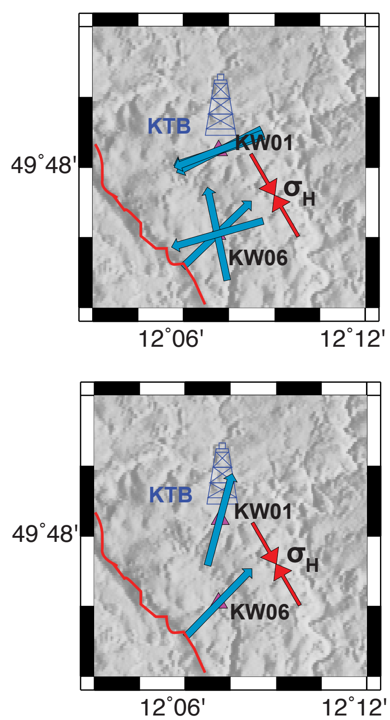
KTB
KW01
σH
KW06
49˚48'
12˚06'
12˚12'
KTB
KW01
σH
KW06
49˚48'
12˚06'
12˚12'

#DATE	OT	LON	LAT	M
2012/07/12	12:51:58	45.45	151.66	5.8
2012/07/20	06:10:25	49.41	155.91	6
2012/07/20	06:32:56	49.35	156.13	5.8
2012/07/25	00:27:45	2.71	96.04	6.4
2012/07/26	05:33:33	-17.59	66.39	6.7
2012/07/29	09:20:55	47.38	139.07	5.6
2012/07/29	12:22:11	14.19	-92.29	5.9
2012/08/02	09:38:30	-8.41	-74.26	6.1
2012/08/10	18:37:43	52.63	-167.42	6.2
2012/08/14	02:59:38	49.8	145.06	7.7
2012/08/18	09:41:52	-1.32	120.1	6.3
2012/08/21	17:39:38	-0.17	92.06	5.6
2012/08/25	14:16:17	42.42	142.91	5.9
2012/08/26	15:05:37	2.19	126.84	6.6
2012/08/27	04:37:19	12.14	-88.59	7.3
2012/08/29	19:05:11	38.42	141.81	5.5
2012/08/31	12:47:33	10.81	126.64	7.6
2012/08/31	23:37:58	10.39	126.72	5.6
2012/11/22	13:07:10	-22.8	-63.69	5.8
2012/11/28	03:09:49	-4.5	-76.12	5.6
2012/12/01	08:00:57	58.67	-154.44	5.7
2012/12/07	08:18:23	37.92	144.02	7.3
2012/12/07	22:59:57	37.77	143.78	5.6
2012/12/14	10:36:01	31.19	-119.6	6.4
2012/12/15	04:49:29	52.27	174.06	6
2013/01/05	08:58:19	55.28	-134.67	7.5
2013/01/08	07:51:31	40.29	142.22	5.5
2013/01/21	22:22:51	4.98	95.97	6
2013/02/02	14:17:34	42.79	143.17	6.9
2013/02/09	14:16:07	1.17	-77.41	7
2013/02/13	03:57:47	30.31	131.4	5.5
2013/02/16	04:37:35	5.96	125.85	6.2
2013/02/22	12:01:59	-27.89	-63.18	6.1
2013/02/25	07:23:56	36.9	139.24	5.7
2013/02/28	14:05:52	50.92	157.36	6.8
2013/03/01	12:53:54	50.97	157.56	6.3
2013/03/01	13:20:52	50.92	157.53	6.5
2013/03/07	03:36:46	24.31	121.49	5.5
2013/03/09	14:56:29	50.89	157.29	5.8
2013/03/24	04:18:34	50.72	160.19	6
2013/03/25	23:02:14	14.7	-90.32	6.2
2013/03/27	02:03:20	23.84	121.13	6
2013/03/31	07:46:18	39.12	141.88	5.5
2013/04/01	18:53:17	39.58	143.1	6
2013/04/03	16:35:46	19.3	95.72	5.6

2013/04/05 13:00:01 42.8 131.08 6.2
2013/04/06 00:29:55 42.79 130.93 5.8
2013/04/10 20:20:27 20.8 122.07 6
2013/04/12 20:33:17 34.4 134.84 5.8
2013/04/17 08:57:24 34.18 139.46 5.7
2013/04/17 12:03:31 38.53 141.56 5.9
2013/04/19 03:05:52 46.26 150.85 7.2
2013/04/19 19:58:40 50.07 157.45 6.1
2013/04/20 13:12:52 50.12 157.13 6.1
2013/04/20 13:18:08 50.03 157.43 5.6
2013/04/21 03:22:17 29.96 138.96 6.2
2013/04/22 01:16:38 18.23 -102.05 6.1
2013/04/29 13:01:42 35.76 140.97 5.5
2013/05/10 19:56:05 -29.16 -13.21 5.8
2013/05/12 07:30:03 13.62 -91.34 5.8
2013/05/12 20:06:45 52.56 -171.98 5.7
2013/05/12 22:42:45 43.98 147.85 5.6
2013/05/14 00:32:26 18.82 145.26 6.8
2013/05/18 04:05:44 -53.16 22.19 5.7
2013/05/18 05:48:01 37.79 141.51 6
2013/05/19 18:44:09 52.29 160.18 5.9
2013/05/19 22:40:28 52.34 159.76 5.7
2013/05/20 23:01:25 52.43 160.24 5.6
2013/05/21 01:55:04 52.44 160.48 6
2013/05/21 03:05:50 52.4 160.38 5.8
2013/05/21 03:08:22 52.43 160.02 5.8
2013/05/21 04:59:37 52.28 160.19 5.6
2013/05/21 05:43:21 52.34 160.01 6.1
2013/05/21 08:25:54 23.5 123.73 5.5
2013/05/21 14:51:19 52.57 160.65 5.6
2013/05/24 05:44:48 54.91 153.34 8.3
2013/05/24 14:56:31 52.26 151.54 6.7
2013/05/27 20:22:04 52.33 160.15 5.5
2013/06/02 05:43:04 23.79 121.08 6.2
2013/06/04 11:00:07 45.44 150.95 5.5
2013/06/04 11:01:57 45.4 151 5.5
2013/06/07 16:38:04 24.08 122.57 5.7
2013/06/13 16:47:23 -9.96 107.27 6.7
2013/06/15 17:34:28 11.52 -87.2 6.5
2013/06/16 05:19:02 18.36 -99.02 6.1
2013/06/27 08:38:09 1.16 127.17 5.7
2013/06/28 23:51:48 24.08 122.36 5.5
2013/07/02 07:37:03 4.72 96.57 6.1
2013/07/03 03:37:32 51.43 -166.86 5.6
2013/07/03 03:40:26 51.51 -167.01 5.7
2013/07/06 05:05:08 -3.26 100.53 6

2013/07/16 14:09:27 43.06 145.45 5.5
2013/07/17 02:37:43 -15.64 -71.81 6
2013/07/20 06:06:23 36.21 141.82 5.6
2013/07/22 07:01:42 -46.16 34.85 6.3
2013/08/04 03:28:51 38.26 141.81 5.8
2013/08/04 15:56:34 47.02 145.3 5.8
2013/08/12 09:49:32 -5.43 -81.97 6.2
2013/08/13 15:43:14 5.78 -78.23 6.6
2013/08/17 16:32:31 -34.92 54 6.1
2013/08/21 12:38:32 17.06 -99.34 6.2
2013/09/05 12:29:18 10.63 -86.07 5.9
2013/09/07 00:19:00 14.77 -92.01 6.5
2013/09/14 15:42:44 51.61 -174.75 6
2013/09/15 16:21:39 51.69 -174.74 6.2
2013/09/25 13:58:15 52.94 171.3 5.5
2013/09/25 16:42:43 -15.91 -74.63 7
2013/09/26 06:46:05 14.45 -93.36 5.7
2013/10/01 03:38:21 53.17 152.88 6.7
2013/10/12 02:10:29 10.86 -62.37 6
2013/10/13 17:32:46 4.04 95.96 5.6
2013/10/15 00:12:33 9.92 124.1 7.1
2013/10/19 17:54:58 26.37 -110.17 6.5
2013/10/24 17:57:35 14.28 93.16 5.5
2013/10/25 17:10:17 37.22 144.69 7.1
2013/10/27 18:13:06 37.21 144.62 5.6
2013/10/31 12:02:08 23.57 121.47 6.3
2013/11/09 22:37:51 35.95 140.03 5.6
2013/11/12 07:03:51 54.81 162.09 6.4
2013/11/19 13:32:55 2.71 128.43 6.1
2013/11/25 05:56:50 45.65 151.03 5.9
2013/12/07 07:36:26 56.85 -155.22 5.7
2013/12/08 17:24:54 44.5 149.17 6.1
2014/01/16 07:33:11 51.33 -179.19 5.8
2014/02/18 23:35:58 -14.23 -75.72 5.9
2014/02/26 21:13:39 53.7 -171.86 6.1
2014/03/02 09:37:55 12.59 -87.63 6.2
2014/03/02 20:11:22 27.47 127.32 6.5
2014/03/10 05:18:13 40.73 -124.97 6.9
2014/03/13 13:20:58 51.36 -179.29 5.5
2014/03/13 17:06:50 33.73 131.67 6.3
2014/03/16 21:16:29 -19.86 -70.58 6.7
2014/03/17 05:11:33 -19.99 -70.88 6.2
2014/03/19 12:19:27 24.07 122.33 5.7
2014/03/21 13:41:08 7.69 94.2 6.4
2014/04/01 23:46:47 -19.68 -70.85 8.1
2014/04/02 16:13:28 7.96 -82.37 6

2014/04/02 23:22:48 39.2 141.77 5.5
2014/04/03 01:58:29 -20.28 -70.51 6.5
2014/04/03 02:43:18 -20.43 -70.3 7.6
2014/04/04 01:37:50 -20.61 -70.62 6.2
2014/04/10 23:27:46 12.54 -86.36 6.1
2014/04/11 20:29:15 11.72 -85.98 6.6
2014/04/15 03:57:02 -53.72 8.68 6.8
2014/04/18 14:27:26 17.46 -100.87 7.2
2014/04/21 20:45:23 17.42 120.07 5.5
2014/04/24 03:10:12 49.78 -127.49 6.5
2014/04/28 00:43:51 19.71 120.12 5.5
2014/05/02 09:15:19 37.89 144.26 5.6
2014/05/04 20:18:24 34.84 139.36 6
2014/05/05 11:08:45 19.68 99.78 6.2
2014/05/08 17:00:17 17.33 -100.75 6.4
2014/05/10 07:36:01 17.28 -100.73 6.1
2014/05/13 06:35:24 7.18 -82.37 6.5
2014/05/15 10:16:43 9.41 122.14 6.2
2014/05/18 01:02:28 4.31 92.73 6
2014/05/21 00:21:13 23.71 121.56 5.5
2014/05/21 10:06:15 17.19 -94.88 5.8
2014/05/28 21:15:05 18.13 -68.39 5.8
2014/06/01 10:07:11 2.02 89.78 5.8
2014/06/14 11:11:01 -10.02 91.02 6.5
2014/06/14 17:31:42 39.47 141.04 5.6
2014/06/15 18:19:13 36.65 141.72 5.6
2014/06/15 20:14:51 37.17 141.01 5.6
2014/06/16 06:39:32 1.64 -79.35 5.6
2014/06/23 20:53:09 51.85 178.76 7.9
2014/06/24 03:15:40 52.26 176.87 6.6
2014/06/24 08:12:32 52.28 176.59 5.7
2014/06/29 05:56:30 24.39 142.64 6.2
2014/06/30 19:55:33 28.39 138.9 6.2
2014/07/03 02:56:38 55.31 166.84 5.7
2014/07/03 12:05:22 55.27 166.97 5.8
2014/07/04 22:42:04 39.72 142.04 5.7
2014/07/05 09:39:31 2.03 97.08 6
2014/07/07 11:23:58 14.88 -92.3 6.9
2014/07/08 09:05:23 42.7 141.47 5.5
2014/07/11 19:21:59 37.06 142.54 6.5
2014/07/14 08:00:01 5.75 126.57 6.3